



CHORUS

This is the accepted manuscript made available via CHORUS. The article has been published as:

Pressure impact on the structure, elasticity, and electron density distribution of CaSi_2O_5

Yonggang G. Yu, Ross J. Angel, Nancy L. Ross, and G. V. Gibbs

Phys. Rev. B **87**, 184112 — Published 21 May 2013

DOI: [10.1103/PhysRevB.87.184112](https://doi.org/10.1103/PhysRevB.87.184112)

The pressure impact on the structure, elasticity and electron density distribution of CaSi_2O_5

Yonggang G. Yu^{1,*}, Ross J. Angel², Nancy L. Ross³, and G. V. Gibbs³

¹ *Institute of Geosciences, University of Frankfurt, Altenhöferallee 1, 60438 Frankfurt a.M., Germany*

² *Dipartimento di Geoscienze, Università di Padova, Via Gradenigo 6, 35131 Padova, Italy and*

³ *Department of Geosciences, Virginia Polytechnic Institute and State University, Blacksburg, VA 24060, USA*

(Dated: April 22, 2013)

Ab initio molecular dynamics simulations were used to reveal the mechanism of the five-fold to six-fold transition in Si coordination numbers of CaSi_2O_5 . The longest first-neighbor Si-O distance drops from 2.8 to 1.8 Å upon the triclinic to monoclinic transition. We find significant bulk modulus softening during the structure crossover, which is due to appearance of intermediate Si-O connections in the triclinic phase under slightly non-hydrostatic stress. Nonetheless, no soft phonon modes were found in either structure, indicating that both structures are dynamically stable. Across the transition, c_{33} doubles and c_{35} increases by six-fold in magnitude due to the formation of new Si-O bonds. Chemical bonding analysis reveals distinctions in the electron localization function and bond ellipticity between the regular (1.8 Å) and the dangling Si-O bonds (2.8 Å), both of which suggest an impending disassociation of the dangling Si-O bond.

PACS numbers:

Keywords: pressure-induced transition; amorphization; pentacoordinate silicon; SiO_5 ; elasticity; spontaneous strain; bulk softening, electron density distribution; electron localization function

I. INTRODUCTION

The discovery of coexisting five-fold and six-fold coordinated silicon atoms in the triclinic polymorph of CaSi_2O_5 ¹ opened the opportunity to explore in a crystalline material one of the critical steps in the process of pressure-induced amorphization, a phenomenon of wide interest found in materials including ice, silica (SiO_2)^{2,3}, AlPO_4 ⁴ and zeolites. An amorphous phase, which lacks long range atomic order (LRO), is thought to be metastable and non-ergodic because its energy landscape exhibits multiple local minima⁵. One viable path for amorphization is elastic and/or vibrational instabilities that destabilize crystal structures; for example, close to amorphization, LRO sharply reduces to zero and a wide range of low frequency vibrational modes arise in phonon spectra. As a result, sharp contrasts may occur in amorphous solids including changes in volume, density, mechanical properties (elasticity), electrical (resistivity) and optical properties. Amorphous materials, such as AlPO_4 , have been shown to possess a “memory” that preserves its crystalline structure and lattice orientation when decompressed from its high-pressure amorphous state⁴. More recently phase change materials (PCM) like $\text{Ge}_2\text{Sb}_2\text{Te}_5$ (GST) have found interesting applications as programmable memory bits, capable of reversibly switching between amorphous and crystalline structures at a remarkably low electric power consumption⁶. In structural biology, organisms can utilize biogenic amorphous calcium carbonate (ACC) as a transient precursor phase to build crystals of desired shapes and polymorphs (calcite and aragonite), such as for mollusk shells⁷. Amor-

phous materials are ubiquitous in meteorites in which they are formed by shock-induced amorphization, and can be produced in laboratory controlled high-pressure devices such as diamond-anvil cells. There were once speculations associating the amorphization of serpentine, a hydrous mineral in subducting lithosphere, with deep-focus earthquakes (100 to 660 km depth) in the mantle⁸.

The fascinating phenomena arising from amorphization transformations have stimulated intensive studies in the field, including structural characterizations using x-ray and neutron diffraction, Raman and infrared spectroscopy, and large scale molecular dynamics simulations. Although previous studies on ZrW_2O_8 ⁹, a well-known flexible framework structure that contracts when heated, have shed light on the problem by suggesting the connection between amorphization and negative thermal expansion, the detailed mechanism of amorphisation is in general still not well understood. In particular, while it is clear that the incipient step of the amorphization in which LRO breaks must involve the breakdown and reformation of chemical bonds, we do not know how this happens. How this incipient process proceeds is also critical for understanding the precursor steps for melting, crystallization and vitrification as well as atom diffusion in melts.

In this study we approach this problem from a different angle. There exists in nature a crystalline material CaSi_2O_5 which is a unique system for studying the incipience of amorphization, because the two polymorphs of CaSi_2O_5 convert into each other reversibly at moderate pressure (0.2 GPa) and stress conditions and, in conjunction, a silicon-oxygen (Si-O) bond switches on (~ 1.8 Å) and off (~ 2.8 Å) when conversions occur.

1 This remarkable material permits a comprehensive the-
 2 oretical investigation on the Si-O bond formation and
 3 rupture in crystalline phases, their influence on elasticity
 4 and structural stability, the quantum mechanical nature
 5 of the regular and elongated Si-O bonds, and the impli-
 6 cations for amorphization. It also allows us to explore
 7 whether the assumption of conventional crystal chem-
 8 istry that such a long Si-O distance is completely non-
 9 bonded is valid. However, since their first unambiguous
 10 characterization through single-crystal x-ray diffraction
 11 experiments¹, only limited efforts have been devoted to
 12 understanding this system. For example, Warren et al.¹⁰
 13 have analyzed covalent bond populations through Mul-
 14 liken analysis and postulated a phase transition path
 15 that interpolates between the five-fold and six-fold co-
 16 ordinated structures. Downs et al.¹¹ have studied bond
 17 critical point properties in CaSi_2O_5 and pointed out a
 18 large bond ellipticity in the lengthened Si-O bond (2.8
 19 Å), denoting the impending rupture of this bond. The en-
 20 thalpy of formation for the transition was measured from
 21 calorimetry¹². Here we focus on the transition mecha-
 22 nism at the atomic scale. We have performed a compre-
 23 hensive first-principles molecular dynamics study on
 24 CaSi_2O_5 , including high-pressure structural simulations,
 25 lattice dynamics, elasticity, and electron density analysis.

26 II. METHOD

27 Our calculation is based on the density functional
 28 calculation¹³ using the Perdew-Burke-Ernzerhof (PBE)
 29 GGA¹⁴ form for the exchange correlation functional
 30 in combination with the plane-wave pseudopotential
 31 method as implemented in the *Quantum ESPRESSO*
 32 package¹⁵. The Troullier and Martins¹⁶ type norm-
 33 conserving pseudopotentials were used for Si, O and Ca.
 34 The accuracy of the Si and O pseudopotentials has been
 35 demonstrated in previous high-pressure studies on the
 36 Mg_2SiO_4 olivine-wadsleyite-ringwoodite system¹⁷ and on
 37 the MgSiO_3 majorite-perovskite-ilmenite system¹⁸. The
 38 PBE-type Ca pseudopotential was generated using a refer-
 39 ence configuration $3s^23p^{4.8}3d^{0.2}$ ($r_c=2.0$ a.u. for s , p ,
 40 and d channels, p local), similar to the recipe of Karki
 41 and Wentzcovitch¹⁹. The non-linear core correction was
 42 not used because of the negligible effect on the equation
 43 of state parameters, a 0.5% increase in volume and a
 44 1% decrease in bulk modulus for CaO. The kinetic en-
 45 ergy cutoff for plane waves (E_{cut}) was chosen to be 80
 46 Ry, and a $2 \times 2 \times 2$ (with $(\frac{1}{2} \frac{1}{2} \frac{1}{2})$ shift from the origin)
 47 Monkhorst-Pack k-point mesh²⁰ was used for Brillouin
 48 zone samplings of the electronic states. Increasing the k-
 49 point mesh to $4 \times 4 \times 4$ and E_{cut} to 90 Ry does not alter
 50 equation of state parameters or the triclinic to the mono-
 51 clinic transition pressure. Crystal structures were relaxed
 52 under hydrostatic pressures using the variable-cell shape
 53 molecular dynamics^{21,22}. The dynamical matrices were
 54 calculated on a $2 \times 2 \times 2$ q -point mesh, and then interpo-
 55 lated to a denser q -point mesh ($4 \times 4 \times 4$) to obtain the

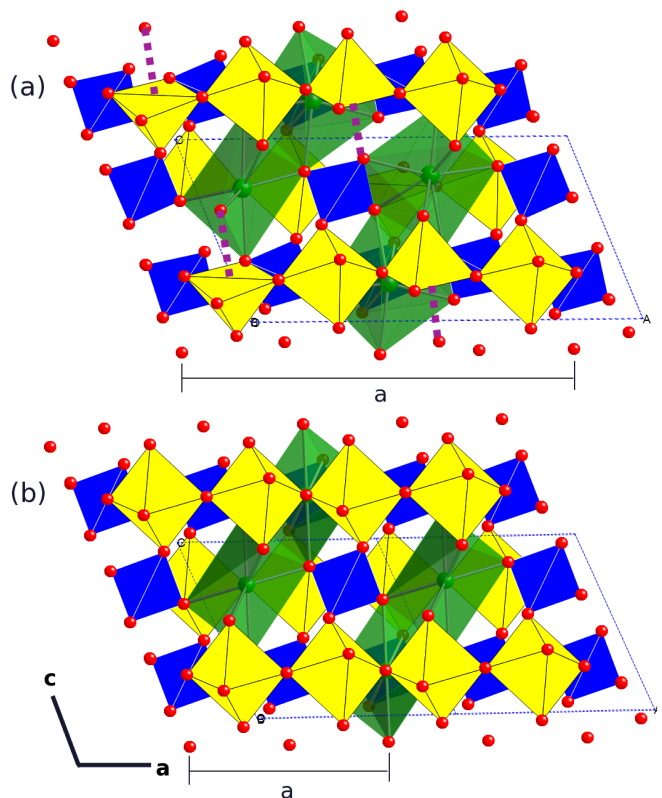


FIG. 1: Crystal structures for the two polymorphs of CaSi_2O_5 : triclinic $\bar{1}1$ (a) and monoclinic $A2/a$ (b). The SiO_5 and SiO_6 units are shown in yellow; SiO_4 tetrahedra are shown in blue; Ca-centered polyhedra are shown in light green; oxygen atoms are shown in red spheres. The dotted lines in (a) denote the hypothetical bonding between Si and O at a distance 2.8 Å. The Ca-O bonds shown here range from 2.2 to 2.5 Å.

phonon density of states.

III. RESULTS AND DISCUSSION

The triclinic CaSi_2O_5 polymorph (space group $\bar{1}1$) was first unambiguously identified by Angel et al.¹ through single-crystal x-ray diffraction. The crystals were obtained by synthesis at high pressures and temperatures, and then quenched to ambient conditions to obtain the triclinic phase. This triclinic structure [Fig. 1(a)] is distinctive for the coexisting four-, five- and six-fold coordinated silicon atoms by oxygen. The tetrahedrally-coordinated silicon atoms cross-link the silicate chains formed by corner-sharing SiO_5 and SiO_6 polyhedra. The pentacoordinate Si atoms are separated 2.8 Å away from the dangling oxygen atoms, in contrast with regular Si-O bonds (1.6 Å in tetrahedral and 1.8 Å in octahedral environments). An experimental study²³ showed that upon compression to 0.2 GPa, each dangling O atom is recaptured by a pentacoordinate Si atom, thus forming

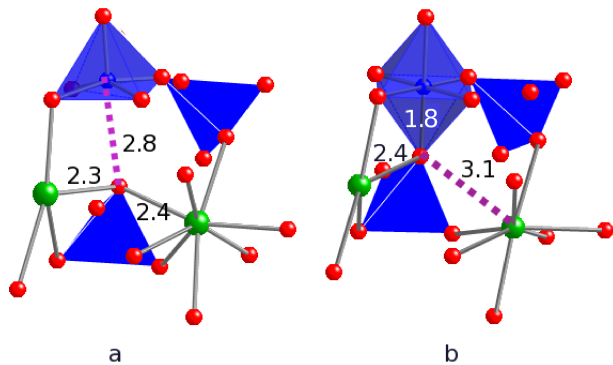


FIG. 2: Polyhedral connectivity in CaSi_2O_5 at 0 GPa from the simulation: (a) the $\bar{1}\bar{1}$ phase and (b) the A2/a phase. The bond lengths that are directly involved in the formation of the ‘sixth’ Si-O bond are indicated. The green spheres represent Ca atoms, blue Si, and red O.

1 an SiO_6 unit. The resulting phase has a monoclinic,
 2 titanite (CaTiSiO_5)-type structure (space group A2/a)
 3 comprising chains of corner-sharing SiO_6 octahedra in-
 4 terconnected through SiO_4 tetrahedra [Fig. 1(b)]. The
 5 reverse transition (six-fold to five-fold coordinate)
 6 was observed in multi-anvil but not in diamond-anvil ex-
 7 periments, which was attributed to the presence of non-
 8 hydrostatic stress in the multi-anvil cell²³. As the rup-
 9 ture of the Si-O bond in CaSi_2O_5 is representative of the
 10 incipient process for amorphization which is commonly
 11 observed in NMR studies²⁴, we use ab initio molecular
 12 dynamics simulations to reveal the microscopic process
 13 underlying the transition which is not accessible experi-
 14 mentally.

15 A. Structural and compressional properties

16 Our simulations confirm that the triclinic phase is ener-
 17 getically more stable than the monoclinic phase at room
 18 pressure. The predicted crystal structure parameters
 19 for the two polymorphs at room pressure are compared
 20 with results from x-ray diffraction measurements in Ta-
 21 ble I. The predicted unit cell lengths and cell angles are
 22 mostly within one-half percent from experimental val-
 23 ues, although GGA overestimates the volume by 1.7 %
 24 and underestimates the bulk modulus by $\sim 10\%$, which
 25 is well known from previous DFT studies on thermody-
 26 namic properties of upper mantle minerals²⁵.

27 The evolution of the triclinic structure towards mon-
 28 oclinic symmetry is simulated using molecular dynam-
 29 ics. This transition is associated with one quarter of sil-
 30 icon atoms changing their formal or apparent coordina-
 31 tion number from five to six. A close view of the local
 32 environment surrounding the dangling oxygen atom at
 33 room pressure (Fig. 2a) shows that it is 2.8 Å away from
 34 Si^{V} (the five-fold coordinated Si) but forms a regular O-

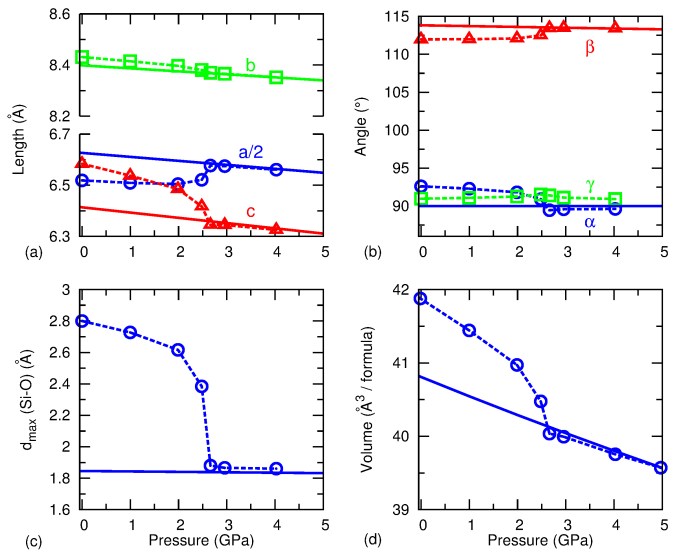


FIG. 3: Variation with pressure of cell parameters — (a) cell lengths, (b) cell angles and (d) cell volumes — across the triclinic (symbols joined by dashed lines) to the monoclinic (solid lines) transition. Also shown is (c) the simulation for the Si-O bond length during its formation process.

35 Si bond (1.61 Å) with Si^{IV} (tetracoordinate Si) and at
 36 the same time it is connected to two Ca atoms in bond
 37 lengths of 2.3 and 2.4 Å, respectively. Upon compression,
 38 the elongated Si-O bond shrinks from 2.8 to 1.8 Å but
 39 one of the Ca-O distances increases from 2.4 to 3.1 Å (the
 40 dashed line in Fig. 2b). This can be interpreted as the
 41 breakdown of the Ca-O bond in favor of forming the short
 42 Si-O bond (1.8 Å). In addition, the Si-O bond formation
 43 is affected not merely from the hopping of the dangling
 44 O atom but involves a translation of the whole SiO_4 unit
 45 towards the pentahedron (see Fig. 2b), indicating the na-
 46 ture of a collaborative transition.

47 Shown in Fig. 3 are the pressure evolution of the crys-
 48 tal structure parameters and that of the elongated Si-O
 49 bond length involved in the transition from GGA calcu-
 50 lations. The open symbols connected by the dashed lines
 51 represent the simulation starting with a triclinic struc-
 52 ture (−4 GPa), whereas the solid straight lines are re-
 53 sults starting from a monoclinic structure at high pres-
 54 sures (10 GPa). When compressed from 0 to 2 GPa, the
 55 cell-parameters of the triclinic phase vary smoothly with
 56 pressure, including cell lengths and cell angles, mean-
 57 while the lengthened Si-O distance decreases from 2.8
 58 Å to 2.6 Å (Fig. 3c). A sudden structural variation oc-
 59 curs, however, between 2 and 2.7 GPa, because multi-
 60 ple competing structures were encountered in the simu-
 61 lation that differ in internal shear stress but have very
 62 close enthalpy, which apparently have prevented the code
 63 from identifying optimal structures that satisfy hydro-
 64 static conditions. This reveals the inability of the tri-
 65 clinic structure to maintain hydrostatic stress with in-
 66 creasing pressures. In addition, no soft phonon modes

1 were found in the triclinic structure even at 2 GPa (see 35
 2 phonon dispersions in the appendix) in the regime in 36
 3 which the structure is showing bulk softening (see below), 37
 4 indicating that the structure with 5-fold coordinated Si 38
 5 is dynamically stable at 2 GPa. This together with the 39
 6 lack of soft phonon modes in the monoclinic structure 40
 7 (the high-pressure phase) from 0 to 5 GPa from this calculation 41
 8 indicates that this transition is not driven by 42
 9 soft phonon modes. What these simulations therefore 43
 10 show, in contrast to the constrained simulations of Warren 44
 11 et al.¹⁰, is that the process is completely reversible 45
 12 and that intermediate structural states, at least up to 2 46
 13 GPa in these simulations, are stable.

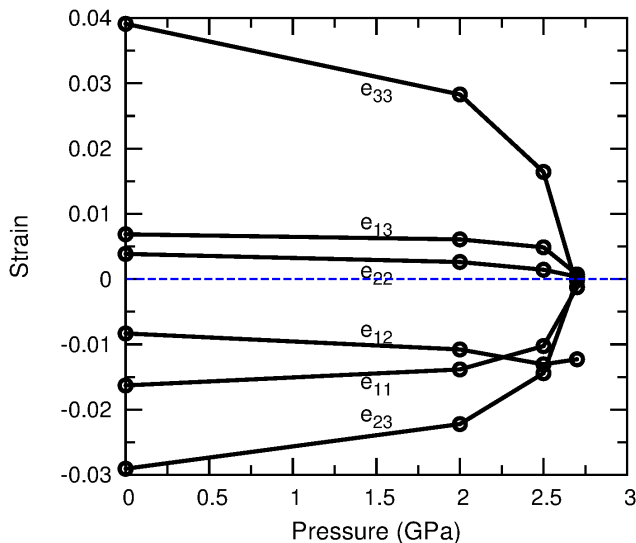


FIG. 4: Spontaneous strains for the low-pressure triclinic structure relative to the high-pressure monoclinic structure in CaSi_2O_5 (for details see appendix).

14 When the pressure exceeds 2.7 GPa, the triclinic phase 15
 16 rapidly converged to the monoclinic titanite structure. The structural parameters at 2.7 GPa are significantly 17
 18 different from those obtained at 2 GPa: the length of the c axis drops from 6.48 to 6.34 Å and that of the a axis 19
 20 increases from 13.0 to 13.15 Å, but the change in the b axis is minute, from 8.40 to 8.37 Å (Fig. 3a). In addition, 21
 22 the β -angle increases abruptly from 112.1° to 113.5°, and the other two angles, α and γ , tend to approach 90° 23
 24 (Fig. 3b). The cause of this dramatic structural change is not just the recovery of the regular Si-O bond (1.8 Å) 25
 26 from the dangling bond state (2.8 Å). The Si-O vector has significant components along both the b and c axes, 27
 28 and so both of these cell parameters decrease. But the formation of the short Si-O bond also increases the intra- 29
 30 chain repulsion resulting in an expansion in the chain length (a axis) and further changes in the cell parameters 31
 32 result from the cooperative rotations of all components of the structure. 33

34 A deeper understanding of the transition mechanism 35
 36 can be gained by plotting the pressure dependence of 37

the components of the spontaneous-strain tensor (e.g., 38
 39 the GGA results) associated with the symmetry-breaking 40
 41 transition (from monoclinic to triclinic, as defined by Eq. 42
 43 38 to 42 in²⁶). The results from Fig. 4 shows the develop- 44
 45 ment of spontaneous strain under decompression. The 46
 47 non-symmetry-breaking strains e_{11} , e_{22} , e_{33} , e_{13} and e_{23} 48
 49 all evolve linearly with one another, as required by sym- 50
 51 metry. At 2.7 GPa, the appearance of the symmetry- 52
 53 breaking strain e_{12} (a non-zero value) corresponds to the 54
 55 discontinuous jump in the γ angle from the simulation (Fig. 3b). At lower pressures, the presence of large axial strains, e_{33} (positive) and e_{11} (negative), correlate with the lengthening of the Si-O bond parallel to the c axis (Fig. 1a), which expands the c axis and shrinks the length of the silicate chains (along the a axis). Similarly the large negative shear-strain e_{23} develops due to the increase in α angle and c axis. The stronger decrease of e_{22} and especially e_{33} compared to the increase in e_{11} as the transition is approached results in a softening of the structure.

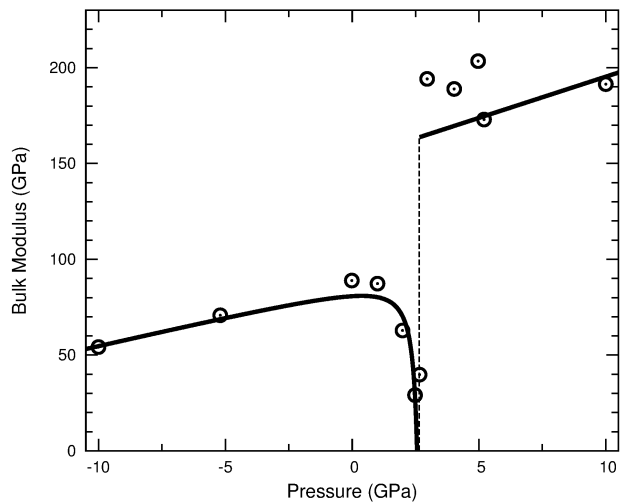


FIG. 5: The calculated bulk modulus of CaSi_2O_5 across the triclinic to monoclinic phase transition. The symbols represent the bulk modulus calculated by finite difference between consecutive P , V data points obtained in simulations. Away from the transition, the lines are the EoS fit to the P - V data of the two phases. In the neighborhood of the transition the line is an interpolation between the data points.

B. Elastic properties

By analyzing the pressure evolution of unit cell volume, we clearly see a structure softening (Fig. 5) accompanying the structure crossover. While at pressures well away from the phase transition the bulk modulus can be described by finite strain equation of state (EoS), there is no adequate method to fit the variation of bulk modulus

1 in the neighbourhood of the transition. We have there-
 2 fore calculated the bulk modulus in this regime by fi-
 3 nite difference between P - V calculated by simulations at
 4 consecutive pressure points. Such a phenomenon is typi-
 5 cal of softening preceding structural phase transitions
 6 at high pressures (e.g.^{27,28}), including softening caused
 7 by spin transitions (e.g.²⁹). As pressure is increased to-
 8 wards the transition, the bulk modulus of the triclinic
 9 phase suddenly drops from 95 GPa to nearly zero, before
 10 it bounces back to 163 GPa, the value of the monoclinic
 11 phase. This clearly correlates with the contraction of
 12 the dangling Si-O bond from 2.8 to 1.8 Å. In fact, this
 13 softening is obviously the combined effect of the rapid
 14 contraction and softening of the crystallographic b and
 15 c directions [Fig. 3(a)], and thus the decrease in e_{22} and
 16 e_{33} (Fig. 4), as a result of the cooperative rearrangement
 17 of the structure described above.

18 To understand the influence of Si-O bond formation on
 19 elasticity, we compare the calculated elastic constants of
 20 the two CaSi_2O_5 polymorphs (Table II). Due to struc-
 21 tural similarity, some elastic constants, such as c_{11} , c_{55}
 22 and c_{12} , are close or of the same order of magnitude for
 23 the two polymorphs, as expected, but there are signifi-
 24 cant differences existing between some other elastic con-
 25 stants. For example, the value of c_{33} of the monoclinic
 26 phase is double that of the triclinic phase, c_{35} is six times
 27 greater, and c_{44} is 58% greater. This is clearly due to the
 28 formation of the extra short Si-O bond (~ 1.8 Å) and thus
 29 SiO_6 octahedra, which stiffens the crystal structure along
 30 the c axis resulting in a large c_{33} , meanwhile increases the
 31 response of the axial stress (σ_{33}) to the shear strain in the
 32 a - c plane (e_{13}), producing a much larger c_{35} . It is also
 33 noted that (Table II) the Cauchy relations which hold
 34 for atomic interactions with purely central forces and in
 35 a lattice with inversion symmetry³⁰ are better obeyed in
 36 the triclinic phase than in the monoclinic phase. For ex-
 37 ample, the ratios $c_{23} : c_{44}$, $c_{13} : c_{55}$, and $c_{12} : c_{66}$, which
 38 equal one according to Cauchy relations, are 0.81 (0.23),
 39 0.83 (0.71), and 1.5 (2.7) in the triclinic (monoclinic)
 40 case, respectively.

41 C. Electron density analysis

42 Here we discuss features of electron density distri-
 43 butions around the regular octahedral and pentahedral
 44 sites, and correlate structure stability with chemical
 45 bonding. The polarization of the Si atoms in the tri-
 46 clinic phase is revealed by the Born effective charge ten-
 47 sors. The Z_{33} components of Si in the tetrahedral, pen-
 48 tahedral, and octahedral environments are 3.18, 3.64,
 49 and 4.17, respectively (Table III), suggesting that the
 50 effective charge transfer amount from Si^{V} to the dan-
 51 gling oxygen atom is indeed much weaker than from Si^{VI}
 52 to its regular oxygen vertex. In the language of quan-
 53 tum chemistry, a bond path can be found along the
 54 2.8 Å Si^{V} -O connection, but it differs markedly from
 55 the regular Si^{VI} -O bonds, as shown in Figs. 7(a,b) which

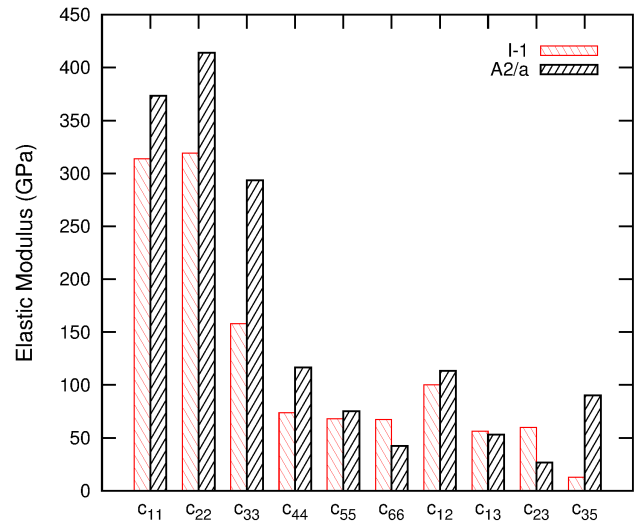


FIG. 6: Comparison of the elastic constants for the triclinic phase (I $\bar{1}$) and the monoclinic phase (A2/a) in CaSi_2O_5 at 0 GPa from the GGA calculation.

compares cross-sections of the valence electron density through the SiO_5 pentahedron and through the regular SiO_6 octahedron. The valence electron density map around Si^{VI} shows a cube-shaped isosurface, which is isotropic towards the six O neighbors [Fig. 7 (b)]. The density around the center of the pentahedron, however, displays a bell-shaped isosurface pointing towards the dangling O atom [Fig. 7 (a)]. At the bond critical point, a local minimum in density along the elongated Si-O path (2.8 Å) is $0.1 \text{ e } \text{Å}^{-3}$, which is much smaller than the minimum density along the regular Si-O bond (~ 1.8 Å) in the octahedral environment, $0.3 \text{ e } \text{Å}^{-3}$. This is consistent with the previous Hartree-Fock all electron calculations¹¹, which shows that the density values at the bond critical points are 0.85 and $0.1 \text{ e } \text{Å}^{-3}$ for the regular and elongated Si-O bonds, respectively. Close to the critical point [Fig. 7 (a)], the density anisotropy perpendicular to the bond path is clearly seen from the asymmetric contour line at $0.1 \text{ e } \text{Å}^{-3}$. A particular measure of this anisotropy is called the bond ellipticity, which is defined as $\epsilon = \lambda_1/\lambda_2$, with λ_1 and λ_2 being the two negative eigenvalues of the Hessian matrix (the second partial derivatives of density with respect to coordinates) at the critical point and in the order of decreasing magnitude. In regular Si-O bonds, $\epsilon \approx 1$, but in the elongated Si-O path it is much larger, 3.55 ¹¹, indicating instability of the bond which is susceptible to rupture.

In addition, the isosurfaces of the electron localization function³¹ calculated from the valence electron density are shown in Fig. 7c. The inner isosurfaces with iso-value 0.85 confines two types of domains: one is shared electron domains represented by small, sphere-shaped density accumulations between bonded Si and O atoms (shown in green lines), and the other is large cone-shaped and

1 torus-shaped domains near O atoms, representing elec- 20
 2 tron lone-pair domains. Clearly, a shared density ac-
 3 cumulation domain exists between all Si^{VI}-O bonds but 21
 4 there is no such feature close to the dangling oxygen atom 23
 5 (Fig. 7c). On the contrary, the localization of the SiO₅ 24
 6 unit appears well defined with the dangling oxygen atom 25
 7 excluded out of their domains as seen from cross-sections 26
 8 of the localization function (Fig. 7d).

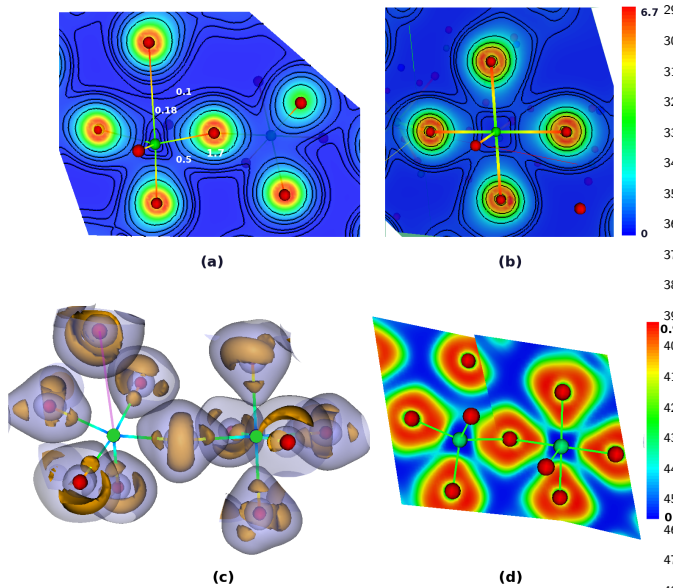


FIG. 7: Chemical bonding for the elongated and regular Si-O 50
 51 bonds in the triclinic CaSi₂O₅ — (a) and (b): the valence
 52 electron density maps; (c) and (d): maps of electron local-
 53 ization function. Si atoms are shown in green spheres and O
 54 atoms in red spheres. (a) A cross-section through the SiO₅
 55 pentahedron containing the dangling Si-O bond of 2.8 Å; the
 56 contour lines for electron density are at 0.1, 0.18, 0.25, 0.5,
 57 0.8, and 1.7 e Å⁻³. (b) A cross-section through a regular SiO₆
 58 octahedron together with the density contour lines at 0.2, 0.3,
 59 0.4, 1.7, 3.35, and 5.0 e Å⁻³. (c) Isosurfaces of the electron local-
 60 ization function of the corner-sharing SiO₅ (left) and SiO₆
 61 (right), with the inner iso-value at 0.85 and the outer at 0.7.
 62 (d) The two cross-sections for the electron localization func-
 63 tion through Si^V (left) and Si^{VI} (right).

9 IV. CONCLUSION 60

10 We have studied in detail the phase transition mecha-
 11 nism associated with the triclinic to monoclinic transition 61
 12 in CaSi₂O₅ from first-principles calculations. Our simu- 62
 13 lation revealed a transition path from the low pressure 63
 14 phase to the high pressure phase, along which one quarter 64
 15 of silicon atoms change their coordination number from 65
 16 five to six. Accompanying the increase in the coordina- 66
 17 tion number are a decrease in the Si-O distance from 2.8 67
 18 to 1.8 Å and an increase in the Ca-O distance from 2.4 68
 19 to 3.1 Å. These bond-length variations are interpreted 69

as a result from the competition for the vertex-oxygen 27
 28 atom between the SiO₅ and the CaO₈ units (Fig. 2). In
 29 addition, we emphasize that not only is the transition
 30 accompanied by the displacement of a single oxygen ver-
 31 tex atom, but also by the collective adjustment of ad-
 32 jacent atoms around the SiO₅ pentahedron, such as the
 33 SiO₄ group. Although the experimental study shows that
 34 the triclinic to monoclinic transition is nearly instanta-
 35 neous (within a pressure interval less than 0.04 GPa), the
 36 molecular dynamics simulation suggests the existence of
 37 intermediate structures in which the dangling Si-O dis-
 38 tance can be 2.6 Å (at 2 GPa). The phonon calculations
 39 at 2 GPa show no signs of soft phonon modes. We also
 40 analyzed the spontaneous strain during the monoclinic
 41 to the triclinic transition, and find e_{12} being the only
 42 dominant symmetry-breaking strain, which corresponds
 43 to the discontinuity in the γ -angle upon the transition.
 44 The elasticity calculation shows that c_{33} and c_{35} of the
 45 monoclinic phase is much larger than those of the triclinic
 46 phase. This is well rationalized in terms of structure by
 47 the formation of the short Si-O bond (1.8 Å) in the mono-
 48 clinic phase, in contrast the corresponding Si-O distance
 49 in the triclinic phase is 2.8 Å. To characterize chemi-
 cal bonding properties around SiO₅ pentahedra and SiO₆
 octahedra, we analyzed the valence-electron density and
 the electron localization function of the triclinic struc-
 ture. The elongated Si-O bond is peculiar in that it has
 a small electron density, but an exceptionally large bond
 ellipticity at the bond-critical point, which indicates that
 the bond is weak, and anisotropic in the transverse direc-
 tion, therefore susceptible to rupture. Clear distinction
 is observed from maps of the electron localization func-
 tion between the elongated Si-O bond and the regular
 Si-O bond; a local maximum exist in the latter bond but
 not in the former. Nonetheless, despite the interpreta-
 tion of conventional crystal chemistry that this long Si-O
 distance does not constitute a ‘bond’ our results show
 that in this case there is still weak residual interaction
 between the Si and O, that would presumably be broken
 on further expansion of the structure.

V. ACKNOWLEDGMENTS

This work was supported by NSF grant EAR-1118691
 and in part by the Alexander von Humboldt foundation.
 One of us (YGY) thanks R. M. Wentzcovitch, S. J. Clark,
 and C. J. Pickard for helpful discussions. Computations
 were performed on the Hess cluster at the Geoscience
 Department at Virginia Tech, for which we are obliged
 to the courtesy of Prof. S. D. King and Prof. Y. Zhou.
 Data analysis was supported in part by ERC starting
 grant 307322 to F. Nestola.

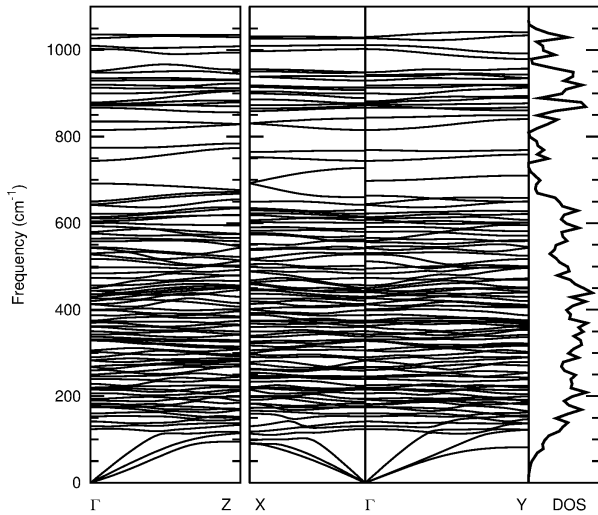


FIG. 8: Phonon dispersions and vibrational density of states of the triclinc CaSi_2O_5 at 2 GPa from GGA calculations. X, Y, and Z denote, respectively, the bisecting points of the three reciprocal vectors: b_1 , b_2 , and b_3 .

VI. APPENDIX

A. Spontaneous strain

We have calculated the bulk and shear moduli for the monoclinic CaSi_2O_5 using the Reuss theory (see e.g.^{32,33}), $K_R = [s_{11} + s_{22} + s_{33} + 2(s_{12} + s_{13} + s_{23})]^{-1}$ and $G_R = 15[4(s_{11} + s_{22} + s_{33}) - 4(s_{12} + s_{13} + s_{23}) + 3(s_{44} + s_{55} + s_{66})]^{-1}$, with the tensor notation denoted in³⁴. We have adopted the notion from Carpenter et al.²⁶ to calculate the spontaneous-strain tensor related to the symmetry-breaking transition from the monoclinic to the triclinc phase (Eq.38 to 42 in²⁶).

B. Phonon dispersions

Phonon dispersions and vibrational density of states of the triclinc structure at 2 GPa from the GGA calculation are shown in Fig. 8.

TABLE I: Crystal cell parameters and equation of states of the two polymorphs of CaSi_2O_5 , the triclinic phase (space group $\bar{1}$) and the monoclinic phase (space group $A2/a$), from the static GGA calculations compared with experiments at room conditions.

Triclinic	$a(\text{\AA})$	$b(\text{\AA})$	$c(\text{\AA})$	$\alpha(^{\circ})$	$\beta(^{\circ})$	$\gamma(^{\circ})$	Vol (\AA^3)	K (GPa)	K'
GGA	13.03	8.43	6.58	92.59	111.96	90.97	670.07	87.0	4.1
Exp ¹	12.917	8.450	6.515	93.161	111.48	90.79	660.32		
Monoclinic	$a(\text{\AA})$	$b(\text{\AA})$	$c(\text{\AA})$	$\beta(^{\circ})$	Vol (\AA^3)	K (GPa)	K'		
GGA	6.63	8.40	6.41	113.82	326.5	152.0	4.0		
Exp ^{2,3}	6.543	8.392	6.342	113.17	320.10	178.2	4		

^{1,1}; ^{2,23}; ^{3,35}

TABLE II: Elastic constants of the monoclinic ($A2/a$) and the triclinic ($\bar{1}$) CaSi_2O_5 at 0 GPa from static GGA calculations, in unit of GPa. The dashed lines represent strictly zero owing to monoclinic symmetry.

C_{ij}	11	22	33	44	55	66	12	13	14	15	16
$A2/a$	373.4	414.1	293.3	116.6	75.0	42.3	113.2	53.0	-	0.0	-
$Im1$	313.7	319.0	158.0	73.8	68.2	67.3	100.0	56.3	3.7	23.4	1.2
C_{ij}	23	24	25	26	34	35	36	45	46	56	
$A2/a$	26.8	-	0.0	-	-	90.0	-	-	0.0	-	
$Im1$	59.8	34.6	-3.1	-4.0	47.9	13.0	-11.1	3.0	10.3	1.2	

TABLE III: Diagonal elements of the Born effective charge tensor of silicon atoms in tetrahedral, pentahedral, and octahedral environment in CaSi_2O_5 (see Fig. 1).

Z_{ij}	Si(IV)	Si(V)	Si(VI)
Z_{11}	3.08	3.90	4.11
Z_{22}	3.48	4.05	3.99
Z_{33}	3.18	3.64	4.17

-
- 1 * Electronic address: yu@kristall.uni-frankfurt.de 37
- 2 ¹ R. J. Angel, N. L. Ross, F. Seifert, and T. F. Fliervoet, 38
3 Nature **384**, 441 (1996). 39
- 4 ² R. J. Hemley, A. P. Jephcoat, H. K. Mao, L. C. Ming, and 40
5 M. H. Manghnani, Nature **334**, 52 (1988). 41
- 6 ³ C. Meade and R. Jeanloz, Science **241**, 1072 (1988). 42
- 7 ⁴ M. B. Kruger and R. Jeanloz, Science **249**, 647 (1990). 43
- 8 ⁵ Y.-T. Cheng and W. L. Johnson, Science **235**, 997 (1987). 44
- 9 ⁶ F. Xiong, A. D. Liao, D. Estrada, and E. Pop, Science **332**, 45
10 568 (2011). 46
- 11 ⁷ S. Weiner, I. Sagi, and L. Addadi, Science **309**, 1027 47
12 (2005). 48
- 13 ⁸ T. Irifune, K. Kuroda, N. Funamori, T. Uchida, T. Yagi, 49
14 T. Inoue, and N. Miyajima, Science **272**, 1468 (1996). 50
- 15 ⁹ T. A. Mary, J. S. Evans, T. Vogt, and A. W. Sleight, Sci- 51
16 ence **272**, 90 (1996). 52
- 17 ¹⁰ M. C. Warren, S. A. T. Redfern, and R. Angel, Phys. Rev. 53
18 B **59**, 9149 (1999). 54
- 19 ¹¹ R. T. Downs, G. V. Gibbs, M. B. Boisen Jr, and K. M. 55
20 Rosso, Phys. Chem. Miner. **29**, 369 (2002). 56
- 21 ¹² M. Schoenitz, A. Navrotsky, and N. Ross, Phys. Chem. 57
22 Miner. **28**, 57 (2001). 58
- 23 ¹³ W. Kohn and L. J. Sham, Phys. Rev. **140**, 1133 (1965). 59
- 24 ¹⁴ J. P. Perdew, K. Burke, and M. Ernzerhof, Phys. Rev. 60
25 Lett. **77**, 3865 (1996). 61
- 26 ¹⁵ P. Giannozzi, S. Baroni, N. Bonini, M. Calandra, R. Car, 62
27 C. Cavazzoni, D. Ceresoli, G. L. Chiarotti, M. Cococcioni, 63
28 I. Dabo, et al., J. Phys. Condens. Matter **21**, 5502 (2009). 64
- 29 ¹⁶ N. Troullier and J. L. Martins, Phys. Rev. B **43**, 1993 65
30 (1991). 66
- 31 ¹⁷ Y. G. Yu, V. L. Vinograd, B. Winkler, and R. M. Wentz- 67
32 covitch, Phys. Earth Planet. Inter. **217**, 36 (2013). 68
- 33 ¹⁸ Y. G. Yu, R. M. Wentzcovitch, V. L. Vinograd, and R. J. 69
34 Angel, J. Geophys. Res. **116**, B02208 (2011). 70
- 35 ¹⁹ B. B. Karki and R. M. Wentzcovitch, Phys. Rev. B **68**, 71
36 224304 (2003).
- ²⁰ H. J. Monkhorst and J. D. Pack, Phys. Rev. B **13**, 5188
(1976).
- ²¹ R. M. Wentzcovitch, Phys. Rev. B. **44**, 2358 (1991).
- ²² R. M. Wentzcovitch, J. L. Martins, and G. D. Price, Phys.
Rev. Lett. **70**, 3947 (1993).
- ²³ R. J. Angel, Am. Mineral. **82**, 836 (1997).
- ²⁴ M. Kanzaki, J. F. Stebbins, and X. Xue, Geophys. Res.
Lett. **18**, 463 (1991).
- ²⁵ R. M. Wentzcovitch, Y. G. Yu, and Z. Wu, in *Theoretical
and Computational Methods in Mineral Physics: Geophysical
Applications, Reviews in Mineralogy and Geochemistry*,
edited by R. M. Wentzcovitch and L. Stixrude (2010),
vol. 71, pp. 59–98.
- ²⁶ M. A. Carpenter, E. K. H. Salje, and A. Graeme-Barber,
Eur. J. Mineral. **10**, 621 (1998).
- ²⁷ J. D. C. McConnell, C. A. McCammon, R. J. Angel, and
F. Seifert, Z. Kristallogr. **215**, 669 (2000).
- ²⁸ B. Mihailova, R. J. Angel, A.-M. Welsch, J. Zhao, J. En-
gel, C. Paulmann, M. Gospodinov, H. Ahsbahs, R. Stosch,
B. Güttler, et al., Phys. Rev. Lett. **101**, 017602 (2008).
- ²⁹ Z. Wu, J. F. Justo, C. R. S. da Silva, S. de Gironcoli, and
R. M. Wentzcovitch, Phys. Rev. B **80**, 014409 (2009).
- ³⁰ M. Born and K. Huang, *Dynamical theory of crystal lat-
tices*, International series of monographs on physics (Ox-
ford at the Clarendon Press, 1956).
- ³¹ A. D. Becke and K. E. Edgecombe, J. Chem. Phys. **92**,
5397 (1990).
- ³² R. Hill, Proc. Phys. Soc. London, Sect. A **65**, 349 (1952).
- ³³ R. J. Angel, J. M. Jackson, H. J. Reichmann, and
S. Speziale, Eur. J. Mineral. **21**, 525 (2009).
- ³⁴ J. F. Nye, *Physical properties of crystals: their represen-
tation by tensors and matrices* (Oxford University Press,
1985), chap. 6.
- ³⁵ R. J. Angel, M. Kunz, R. Miletich, A. B. Woodland,
M. Koch, and R. L. Knoche, Am. Mineral. **84**, 282 (1999).